LETTER

doi:10.1038/nature13487

An optoelectronic framework enabled by low-dimensional phase-change films

Peiman Hosseini[1], C. David Wright[2] & Harish Bhaskaran[1]

The development of materials whose refractive index can be optically transformed as desired, such as chalcogenide-based phase-change materials, has revolutionized the media and data storage industries by providing inexpensive, high-speed, portable and reliable platforms able to store vast quantities of data. Phase-change materials switch between two solid states—amorphous and crystalline—in response to a stimulus, such as heat, with an associated change in the physical properties of the material, including optical absorption, electrical conductance and Young's modulus[1–5]. The initial applications of these materials (particularly the germanium antimony tellurium alloy $Ge_2Sb_2Te_5$) exploited the reversible change in their optical properties in rewritable optical data storage technologies[6,7]. More recently, the change in their electrical conductivity has also been extensively studied in the development of non-volatile phase-change memories[4,5]. Here we show that by combining the optical and electronic property modulation of such materials, display and data visualization applications that go beyond data storage can be created. Using extremely thin phase-change materials and transparent conductors, we demonstrate electrically induced stable colour changes in both reflective and semi-transparent modes. Further, we show how a pixelated approach can be used in displays on both rigid and flexible films. This optoelectronic framework using low-dimensional phase-change materials has many likely applications, such as ultrafast, entirely solid-state displays with nanometre-scale pixels, semi-transparent 'smart' glasses, 'smart' contact lenses and artificial retina devices.

Phase-change materials (PCMs) have been key to enabling the creation of a versatile platform able to store vast amounts of information on inexpensive plastic substrates (DVDs and other optical media[6,7]) using optical pulses. These technologies use light of specific wavelengths (for example, Blu-Ray at 405 nm, DVDs at 650 nm and CDs at 780 nm) to write and read data. The next generation of electronic, solid-state memories based on PCMs could replace the current leading storage technologies, namely Flash and magnetic disks. PCMs[1–5] have extraordinary properties such as extreme scalability, fast switching speeds, and high switching endurance[4,5]. However, although PCMs have been commercialized in both the electrical[4] and optical domains[8], there has been very little research into understanding how transforming the phase in one domain affects the properties in another (that is, how switching electrically affects optical properties, and vice versa). This is because the likely applications emerging from such non-volatile, optoelectronic properties have so far been unclear. Here we propose and demonstrate these optoelectronic properties in the context of novel display and data visualization applications.

Recently, thin-film perfect absorbers in the mid-infrared part of the spectrum have been demonstrated, where the optical properties of a temperature-transient PCM (vanadium dioxide, VO_2) were tuned[9]. VO_2, however, is stable in each of its phases only within certain temperature ranges, a property that makes it energy inefficient and impractical to implement in electrically controlled circuits at the nanoscale. In contrast, the primary phases of $Ge_2Sb_2Te_5$ (GST)—amorphous and crystalline—are stable for most applications[10] and can be thermally, optically or electrically switched at ultrahigh speed[11,12]. Furthermore, GST is extremely scalable[13,14], easily integrated in commercial devices and has optical properties that can be tuned in the visible spectrum of light[15].

We describe a unique optoelectronic framework technology employing GST-based thin films and experimentally demonstrate its wide-ranging applicability in various types of display technologies. We show how such a system, when combined with a transparent electrode such as indium tin oxide (ITO), can be used as a reflective or a semi-transparent microdisplay and on both rigid and flexible substrates, which could usher in an era of truly flexible electronic screens that can operate at the maximum possible resolution allowed by the diffraction of visible light, both as backlit displays and electronic readers. Current microdisplay technologies based on liquid crystals, microelectromechanical systems and organic light-emitting diodes are attracting considerable attention because of a growing interest in wearable technology[16]. Key requirements for such applications are high resolution, high speed and low power consumption, all of which are met by the technology described here.

We first describe the reflective type of display using GST-based thin films. Figure 1a shows the cross-sectional schematic of our reflective devices; the GST is sandwiched between two ITO layers and deposited on top of a reflective surface such as platinum. The crystallization of the few-nanometres-thick GST layer induces a colour change in the entire film, visible when incident 'white' light is reflected back. To understand the relationship between the thickness of the ITO and GST layers and the overall optical properties of the stack we systematically compute the reflectivity spectra of the stack while gradually increasing the thickness of each layer. Every calculation is made twice, one for each phase of the GST layer; a change in the refractive index of the GST layer (caused by a change in phase) modulates the reflective spectrum of the entire stack. The spectra are finally compared and the percentage change in reflectivity is plotted as $\Delta R\ (\%) = \left(\frac{R_{\mathrm{crystal}} - R_{\mathrm{amorphous}}}{R_{\mathrm{amorphous}}} \times 100 \right)$, with R_{crystal} being the reflectivity (at a specific wavelength) of the entire stack when the GST layer is in the crystalline phase and $R_{\mathrm{amorphous}}$ its reflectivity when the GST layer is in the amorphous phase. We use the above expression because the amorphous phase is the as-deposited phase in our experiments. These models (top graphs in Fig. 1b) indicate that one key factor is the presence of a transparent conductor beneath the GST (with thickness t in Fig. 1a), which we refer to as the ITO spacer. This layer is crucial and contributes to the colour in our system.

To experimentally verify our reflectivity calculations, we sputter a number of multi-layered films on silicon wafers with a 300-nm-thick thermally grown silicon dioxide (SiO_2) layer; our GST layer is known to be amorphous as sputtered (section S4 in the Supplementary Information). Figure 1d shows a photograph of a few sputtered films with similar structure (10 nm ITO/7 nm amorphous GST/t nm ITO/100 nm Pt/SiO_2); t is the only thickness that is varied. The colour of the films when t (the ITO spacer thickness) is varied varies dramatically. To fully crystallize the GST, we heat each sample up to 220 °C for a few minutes on a hot plate. The observed variation in the colour of these samples when the GST is crystallized is also shown in Fig. 1d; the colour variations show the

[1]Department of Materials, University of Oxford, Parks Road, Oxford OX1 3PH, UK. [2]College of Engineering, Mathematics and Physical Sciences, University of Exeter, Harrison Building, North Park Road, Exeter EX4 4QF, UK.

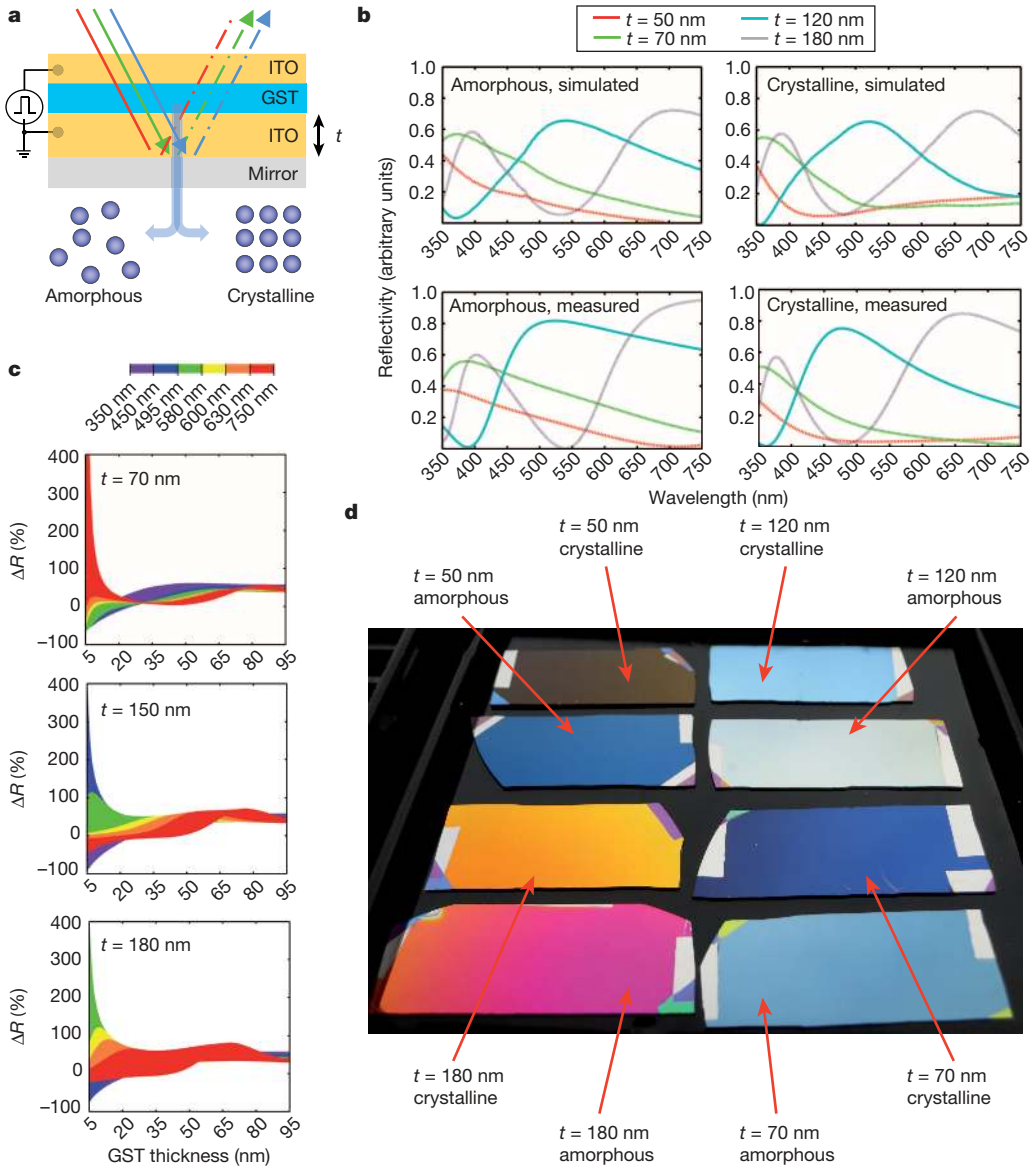

Figure 1 | Colour tunability using ultrathin PCM films. **a**, Schematic representation of the thin-film material stack comprising ITO/GST/ITO. The crystallization of the few-nanometres-thick GST layer induces a colour change in the entire film, visible when incident white light is reflected back. **b**, Simulated (top, left) and measured (bottom left) reflectivity spectra of the amorphous samples together with the simulated (top, right) and measured (bottom, right) reflectivity spectra of the crystalline samples shown in **d**. In both phases, the close match between the model and simulation is striking. **c**, Change in reflectivity simulated for visible wavelengths, for various thicknesses of the ITO spacer and with increasing thickness of the GST layers. Each graph represents the change in optical reflectivity $(R_{crystal} - R_{amorphous})/R_{amorphous} \times 100$ when the PCM embedded in the ITO/GST/ITO/Pt structure is switched from the amorphous to the crystalline phase. By tailoring the thickness of the ITO spacer, the reflectivity of specific wavelengths is enhanced, and the remaining wavelengths are either decreased or weakly increased, when white light is used for illumination. **d**, An example of four different films with similar layered structure (starting from the topmost layer) consisting of 10 nm ITO/7 nm GST/*t* nm ITO/100 nm Pt with different thicknesses of *t*, the ITO layer deposited between the GST and the reflective Pt layer. The value of *t* determines the reflected colour. After the deposition process, one part of each sample is placed on a hot plate at 220 °C for a few minutes to induce complete crystallization of the GST layer. The corresponding colour change is also visible, and is quite dramatic. For example, the white ($t = 120$ nm) amorphous film turns light blue when crystallized. No postproduction colour is added to enhance contrast.

potential for the use of such films as individual pixels in display devices, each pixel being a different colour to achieve a standard colour display device (and with switching in real devices achieved electrically; see below).

To quantify this colour change, we first model the system using a transfer matrix optical computational method[17] to calculate properties such as reflectance, transmittance and internal electrical field at visible wavelengths (full details of the model are available in section S5 of the Supplementary Information). We then carry out reflectivity measurements on sputtered films to compare our model with experiments; we use a spectrometer (Lambda 1050, Perkin Elmer US) to obtain the reflectivity spectra of the samples both before and after crystallization. Figure 1b shows exceptionally good agreement between the simulated (top, left) and measured (bottom, left) reflectivity spectra for the samples shown in Fig. 1d, when the thin GST layer is in the amorphous phase. Similar reflectivity spectra are shown (Fig. 1b, right) for the same samples after crystallizing the GST layer, where again the agreement between experiment and theory is very good. These results show that an effective change in the reflectivity spectrum (that is, colour) of the stack can be induced simply by changing the phase of a chalcogenide layer a few nanometres thick.

The next aspect of our study focuses on the influence of the GST thickness. In conventional optical disks, the thickness of the GST layer is

optimized, along with the thicknesses of surrounding dielectric layers, to enhance the optical contrast. However, the GST thicknesses used in commercial disks are relatively high (several tens of nanometres, typically). In the case of the films shown in Fig. 1d, the thickness of the GST layer is just 7 nm (the very minimum we could sputter reliably using our facilities). Counter-intuitively, as we explain below, smaller thicknesses enhance contrast dramatically and, importantly, lead to lower power electrical switching. Figure 1c shows our computational study of the change (shown as a percentage) in optical reflectivity for various thicknesses of the ITO spacer and with increasing thickness of the phase-change layer. For a thin layer of GST (that is, below 20 nm) the range of wavelengths that show increased reflectivity upon crystallization varies depending on the chosen thickness of the ITO spacer. This allows the perceived colour of the entire stack to be transformed simply by changing the phase of a GST layer a few nanometres thick. Interestingly, this crystallization-induced variation of reflectivity is exponentially amplified for thinner layers of the PCM. Also, by tailoring the thickness of the ITO spacer, the reflectivity of specific wavelengths is enhanced when white light is used as the illumination source. Figure 1c shows three examples with ITO thicknesses of 70 nm, 150 nm and 180 nm where the red, green and blue components, respectively, are enhanced with the remaining wavelengths either decreased or weakly increased. The importance of the ITO spacer is further elucidated in section S7 of the Supplementary Information, where the absence of interference (that is, no ITO spacer is inserted between the GST and the Pt layer) causes the reflectivity of the film to increase only weakly in the crystalline phase, mostly independently of the wavelength.

We now demonstrate how this thin-film stack could be used in future PCM-based display applications. To demonstrate the working principle of a display that can be electrically switched, we pattern an image using a nanometre-sized electrical probe (that is, the conductive tip of an atomic force microscope, CAFM), which was previously shown to be capable of switching nanoscale crystalline areas[18–20] in PCM films. Our technique uses a pixelated approach mimicking real pixels in actual devices (the fabrication of such a device is described below). The use of CAFM to characterize the nanoscale switching characteristics of PCM from the more-amorphous to more-crystalline phase has been studied previously, and is known to closely resemble a standard cross-bar phase-change memory cell; hence, we employ this technique to demonstrate our electrically enabled display technology[18,21]. More details regarding this technique and how it relates to actual PCM-based devices (pixels) can be found in section S1 of the Supplementary Information. To demonstrate the high optical contrast, we start by electrically drawing the Oxford Radcliffe Camera building (the grayscale image of which is shown in Fig. 2b) in Fig. 2c, d and e on similar films with ITO spacer thicknesses of 50 nm, 70 nm and 180 nm, respectively. All the pictures are clearly visible using a standard, non-polarized, optical microscope. No artificial contrast or colour has been added in postproduction. The striking contrast demonstrates the feasibility of such ultrathin PCM-based microdisplays. To demonstrate the colour-rendering capability, a different pattern representing the University of Oxford logo (shown in Fig. 2f) is also electrically drawn on a 20 nm ITO/7 nm GST/70 nm ITO/100 nm Pt stack. The resulting optical image is shown in Fig. 2g, which closely matches the original logo, representing the 'Oxford blue' in Fig. 2f (note the striking contrast between the blue and white regions).

We then verify that a pixelated array, as would be necessary in a display where each pixel can be randomly accessed and manipulated, is approximated very closely by our CAFM approach. To perform this verification, we fabricate an array of 300 nm × 300 nm pixels with 200 nm pitch on a

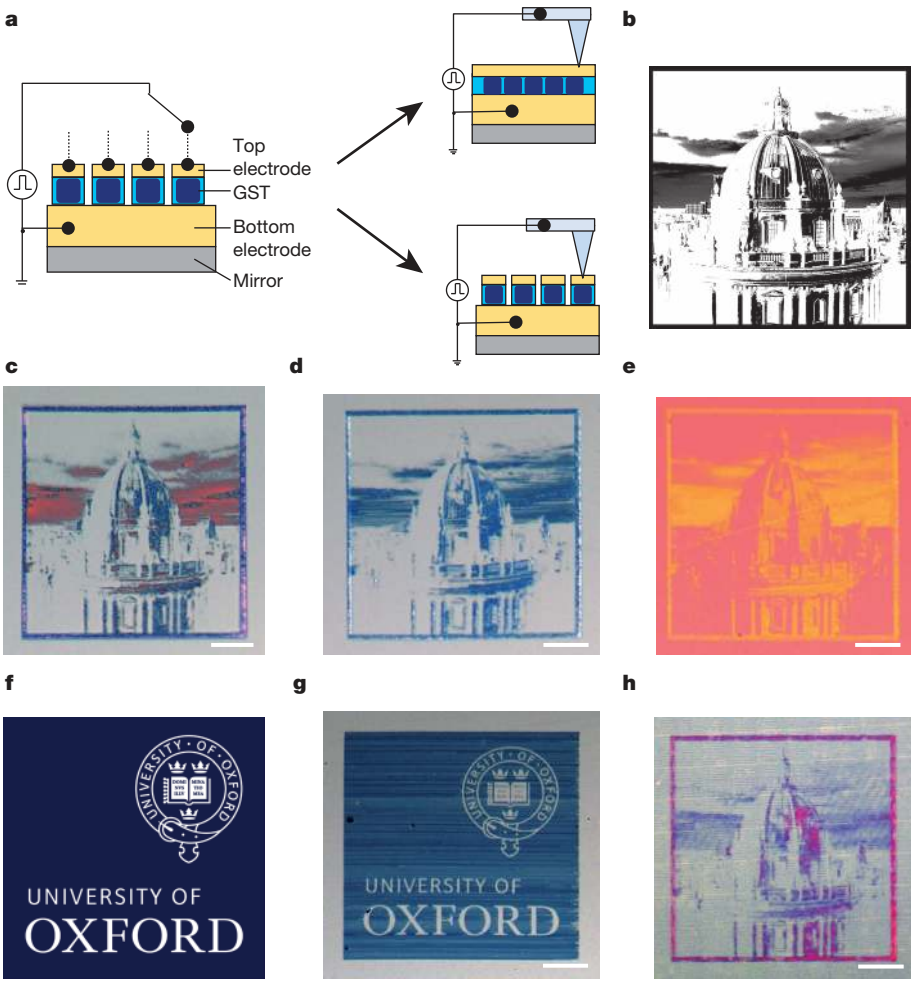

Figure 2 | Reflective display films. **a**, Schematic illustration of the electrically induced colour changes in phase-change-based electronic displays. **b**, The original (greyscale) picture of the Oxford Radcliffe Camera used as a pattern. **c**, Electrically constructed image on a continuous ITO/GST/ITO/Pt stack with a 50-nm-thick ITO spacer; the white regions are regions where the phase is amorphous. No artificial contrast has been added in postproduction. The pattern is once again electrically reproduced on various stacks with ITO spacer thickness of 70 nm (**d**) and 180 nm (**e**). Scale bars are 10 μm, which show the ultimate resolution such displays are capable of achieving. **f**, The original image of the University of Oxford logo is used as a different pattern. **g**, Electrically constructed image on a ITO/GST/ITO/Pt stack with 70-nm-thick ITO spacer—the blue regions are regions where the phase is transformed. **h**, To verify the effectiveness of our blanket film approach we electrically transformed an array of lithographically defined 300 nm × 300 nm pixels (200 nm pitch) on a standard vertical stack with a 50-nm-thick ITO spacer; the optical contrast is strikingly evident, experimentally confirming that the pixelated array is well approximated by a CAFM-generated one.

standard vertical stack with a 50-nm-thick ITO spacer. The active volume of each phase-change cell (that is, the GST layer) is restricted to a single pixel precisely addressable by the nanoscale tip. These pixels were electrically switched using a nanoscale conductive tip. Figure 2h shows the resulting optical image, where the optical contrast is once again striking. Further experiments using electrically switched single pixels, together with the resulting high optical contrast, are shown in section S1 of the Supplementary Information.

We now move on to transparent substrates and electrically modulate their optical transmission. Future semi-transparent displays will find applications in emerging technologies such as contact-lens-type displays[22], 'smart' eye glasses, windshield displays, for modulating light transmission through windows[23] or even for synthetic retina devices[24]. Such light modulation, achievable with resolution beyond the diffraction limit, is also important for future ultrafast phase modulators, where a white light behind the semi-transparent display is selectively diffracted to produce interference. For such a configuration the reflective platinum underlayer is not deposited and the entire structure (ITO/GST/ITO) is sputtered directly on top of a transparent substrate, quartz in our case. As in the previous case of reflective displays, the electrically induced crystallization (and re-amorphization) can be used as a means of creating optical contrast.

Figure 3a shows a schematic of the principle behind semi-transparent, phase-change-based displays. The calculated change in transmission (shown as a percentage) between the amorphous and crystalline phase is shown in Fig. 3b. According to the model, a GST thickness of around 75 nm to 85 nm gives the highest change in transmission for most wavelengths. However, owing to the intrinsic absorption of the GST layer, the opacity of the films quickly drops after a few nanometres (see section S6 of the Supplementary Information). We therefore choose a 7 nm GST layer sandwiched between a 20-nm-thick ITO and a 40-nm-thick ITO as the best compromise between contrast and transparency. We also confirm the calculated change in absorption and transmission characteristics of such a film (shown in Fig. 3c) by measuring and comparing its transmission (or absorption) spectra upon crystallization.

We use the CAFM (similar to the experiments on reflective substrates) to render pixelated images on these substrates. Figure 3e shows an example of an electrically constructed image on such a substrate. To illustrate the transmissivity of the substrate, a square green pad is placed underneath the rendered image; the transmissivity modulation is visible in Fig. 3d and 3e (the logo of Wolfson College, University of Oxford) and the contrast and transparency of the electrically drawn image is clear. This demonstrates the principle of using such phase-change optoelectronic frameworks for transmissive micro- and nanodisplay applications, from electronic displays on windows, to backlit displays and as future wavelength-tuneable windows.

Finally, given the extremely low thickness of our films, we find that they are amenable to flexible films (and therefore flexible displays). The development of a low-power, ultrathin flexible display has been a long-term goal worldwide, and the use of ITO could enhance the possibility of using them as touch-sensitive displays. Figure 4a shows a picture of a 20 nm ITO/7 nm GST/50 nm ITO/100 nm Pt multi-layered film on biaxially oriented polyethylene terephthalate (boPET). The flexibility of these films with the sputtered layers is demonstrated in Fig. 4a, c and d. The colour variation in these flexible reflective displays is entirely similar to that on rigid substrates (Fig. 2). Again, we render images using a

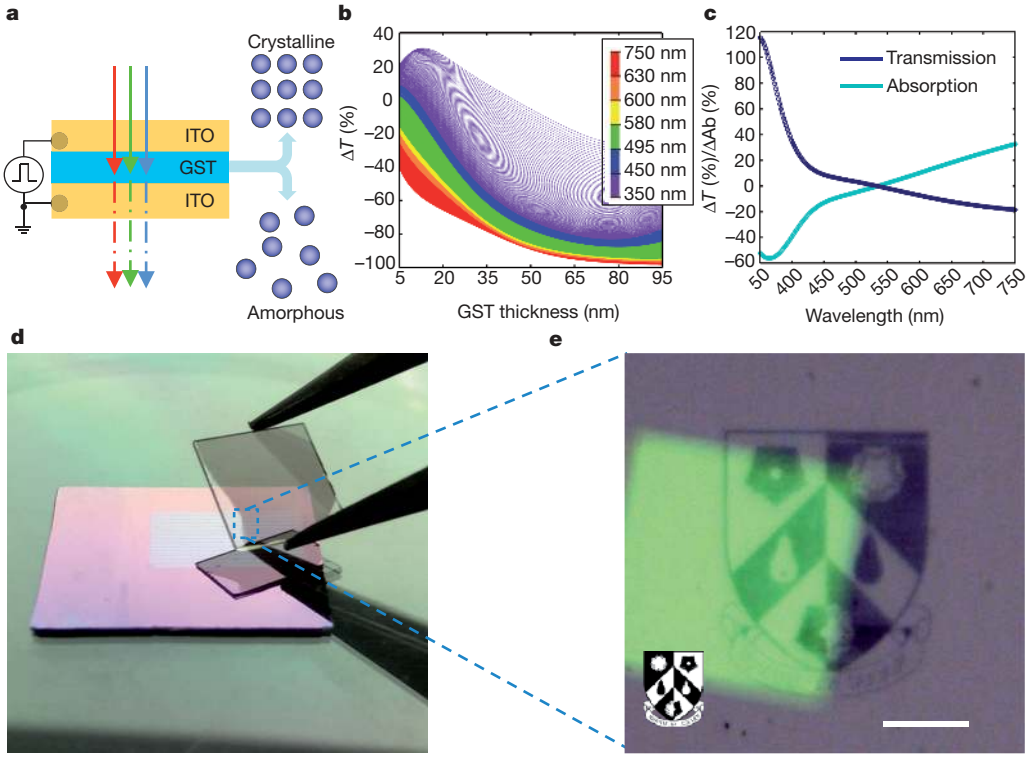

Figure 3 | Semi-transparent display type films. **a**, Schematic diagram of the principle behind a semi-transparent device using a ITO/GST/ITO structure on quartz. **b**, Computed change in optical transmission $\Delta T(\%) = \left(\frac{T_{\text{crystal}} - T_{\text{amorphous}}}{T_{\text{amorphous}}} \times 100\right)$, at different wavelengths, when the GST layer is switched between the amorphous and crystalline phases. **c**, Measured change, upon crystallization, in absorption $\Delta\text{Ab}(\%) = \left(\frac{\text{Ab}_{\text{crystal}} - \text{Ab}_{\text{amorphous}}}{\text{Ab}_{\text{amorphous}}} \times 100\right)$ and transmission spectra of a 20 nm ITO/7 nm GST/40 nm ITO film sputtered on quartz. **d**, A picture of the film measured in **c**. **e**, Microscope picture of an electrically constructed image on the film, demonstrating the principle of semi-transparent PCM-based electronic paper displays. The green sample pad visible underneath the image demonstrates the semi-transparent nature of the thin-film layers and enhances clarity (because of the finite thickness of our transparent substrate, it is not in focus). The scale bar is 50 μm, highlighting the high resolution that is possible.

nanoscale conductive probe, and the resulting image is shown in Fig. 4b. Although the quality of the boPET substrate is much inferior to that of semiconductor-grade SiO_2 or quartz, the electrically written high-resolution image of the Oxford Radcliffe Camera is readily visible. Another example of a similar film with a 180-nm-thick ITO spacer is shown in Fig. 4c, where the colour is now closer to yellow, which shows the range of possible colours. Thus the use of such flexible films in semi-transparent modes is also possible. It is also remarkable that there is no visible colour variation when the films are bent, suggesting that such thin films also can be used as wide-viewing-angle displays. A semi-transparent, flexible film is shown in Fig. 4d, completing the demonstration for reflective and semi-transparent type displays on rigid, flexible and transparent substrates.

In all the above examples we use a CAFM to electrically switch the GST sandwiched between two ITO layers. Because no device using ITO electrodes has yet been demonstrated, we show that such a device (a single pixel) can be made and switched. Using a combination of electron beam lithography, reactive ion etching and sputtering deposition, we fabricate vertical, crossbar-like ITO/GST/ITO devices to test their electrical switching characteristics. We fabricate these devices on 300-nm-thick SiO_2 on silicon substrates (see section S3 of the Supplementary Information for fabrication details, and section S1 for the use of ITO as active electrode). An optical image of a few crossbar devices is shown in Fig. 5a with a false-colour magnified scanning electron microscopy image of one such device in the inset. This particular device has an active area (defined by the area of overlapping crossbars) of 300 nm × 300 nm. We note that switching in phase-change memories is often restricted to nanometric regions of the cell[25]. The use of nanoscale devices (pixels) is therefore preferable, since full crystallization and re-amorphization of the pixel is required to enhance these novel optoelectronic functionalities. The electrical switching characteristics of such devices have been tested for various test cells with an example shown in Fig. 5b and c. This particular cell shows a threshold voltage[26] of 2.2 V with a 350× increase in conductance between the amorphous and crystalline phases. Figure 5b shows a collection of direct-current (d.c.) current–voltage curves used to transform the device to the high-conductance (low resistance or crystalline phase) state (referred to in PCM devices as the SET state). 100-ns pulses with a fall-time of 5 ns and amplitude of 5 V are used to transform the device to its initial low conductance (high resistance or amorphous) state (referred to as the RESET state in PCM devices). A collection of SET/RESET iterations is shown in Fig. 5c demonstrating its repeatability (the cycle endurance of our devices will require further engineering to create a commercial system, but we note that commercial-type phase-change memories with endurances of greater than 10^8 cycles have been demonstrated[27]). It is clear that our device is a single pixel (of very high resolution), and it is reasonable to expect that such a pixel can be replicated for display applications.

We now address the energy requirements for such a display using the results obtained from the single pixel device. In phase-change memories the highest energy consumption is in the re-amorphization of a cell where sufficient energy is required to melt the PCM[4]. We estimate the energy required to re-amorphize a single ITO/GST/ITO cell to be 15 pJ, on the basis of our experimental results. A 300-cm^2 display with 200-nm cell size and a 50-nm gap between each cell would thus require 7.2 J to completely re-amorphize, similar to electrochromic devices[28]. The development of even thinner PCM would enable the energy consumption of a device (pixel) to be drastically reduced by ten to a hundred times[13], which would also increase the optical contrast, as already discussed. This would enable the use of phase-change-based electronic paper also as dynamic displays with few constraints on power requirements and ultrahigh (in the megahertz range) switching speed. Crucially for power consumption, no energy is required after a switching event, giving net zero-power consumption in static mode, a further improvement over existing colour back-lit microdisplays.

Such cells can thus be fabricated, are reliable and can be switched reversibly with low power. Many challenges remain, especially in understanding how larger pixels can be switched most effectively and yet display optical contrast, as well as in arraying and subdividing pixels effectively to create any arbitrary colour and greyscale. The use of growth-dominated PCMs may prove to be a very useful approach in this respect, although

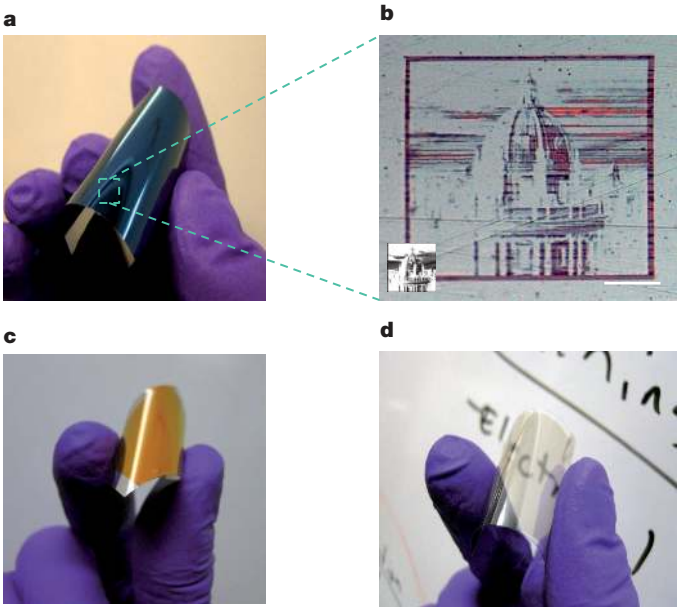

Figure 4 | Flexible display films in both reflective and semi-transparent mode. **a**, Reflective device on boPET, showing flexibility as well as the wide-viewing-angle colour consistency of such films (that is, when the film is bent, the colour in the bent region is not dramatically different). **b**, An electrically defined image is patterned directly on top of the flexible substrate using a CAFM. **c**, Another example of a reflective stack. **d**, A semi-transparent type structure sputtered directly on a flexible boPET substrate.

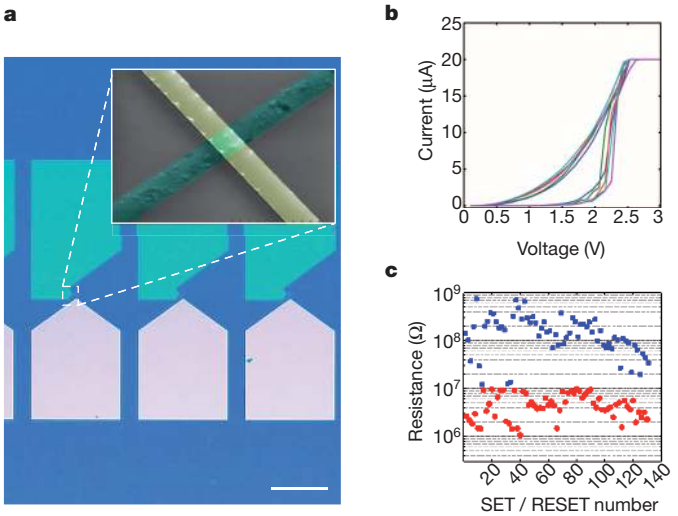

Figure 5 | Demonstration of a single pixel. **a**, Optical image of a few ITO/GST/ITO crossbar-like devices, with a false-colour scanning electron micrograph of one single device in the inset. The scale bar is 100 μm. **b**, A collection of various current–voltage curves demonstrating the amorphous-to-crystalline switching behaviour of several ITO/GST/ITO cells. These devices display a threshold voltage of approximately 2.2 V with a decrease in resistance of about 350× when switched from the amorphous to the crystalline phase. The maximum current was limited to 20 μA. **c**, SET/RESET cycling of the same device. Direct-current sweeps (similar to those in **b** above) are used to switch the device from the RESET (high resistance) state to the SET (low resistance) state. Several pulses of 5 V in amplitude with 100 ns width, 20 ns rising and 5 ns trailing edges are used to switch the device back from the SET state to the RESET state.

their optoelectronic properties also remain unexplored and could be the subject of further research in this field.

In conclusion, we have demonstrated a unique optoelectronic framework based on low-dimensional PCM films. The integration of a PCM as an active switching layer in displays paves the way for a new class of 'smart' devices that are both electrically and optically active. Our results represent the first applications of the electro-optical properties of such materials. Very thin layers of PCM can display very high optical contrast upon switching between the amorphous and crystalline phases when layered in appropriately designed thin film structures. Because this can be done electrically, it allows for the fabrication of large arrays to create displays with ultrahigh resolution. We demonstrate such displays on reflective and transparent substrates both on rigid and flexible surfaces; results that promise truly foldable ultralight displays that consume no power in static mode. We then further demonstrate the fabrication of one single pixel of a phase-change cell with transparent electrodes. Because PCMs are also capable of storing data and performing arithmetic and logic, such devices could potentially mimic the functionality of photoreceptor cells in the human eye, opening up new fields of research in human–machine interaction, multi-functional glasses, contact lenses and synthetic retina devices.

METHODS SUMMARY

Film deposition. Films are sputtered directly on thermally grown SiO_2 wafers (IDB Technology, UK), boPET (Mylar) or quartz. Substrates were cleaned for 10 min in acetone under ultrasonic agitation, rinsed in isopropanol and dried with pressurized nitrogen. Where a reflector was needed (reflective devices), 100-nm-thick Pt was deposited using a Nordiko sputtering system: starting pressure 4.7×10^{-7} torr, working pressure 1.6 mtorr, 30 sccm (standard cubic centimetres per minute) Ar, 400 W d.c. 9 r.p.m. The samples were then moved to a second sputtering system for ITO and GST deposition. ITO is sputtered from a solid target (Testbourne, UK) using 25 W direct current, 1.1 mtorr working pressure, 4×10^{-6} torr starting pressure, 100 °C sample temperature at a rate of 2 nm min^{-1}. Substrate heating is found to greatly reduce final surface roughness, increase optical transparency and electrical conductivity. $Ge_2Sb_2Te_5$ is sputtered from a solid target (Super Conductor Materials, USA) at 25 W d.c., 1.1 mtorr working pressure, 4×10^{-6} torr starting pressure and a rate of 8.5 nm min^{-1}, immediately following the ITO deposition in vacuum.

Optical characterization. Films were measured using a Lambda 1050 spectrometer (Perkin Elmer, USA) in reflection, absorption and transmission using wavelengths between 350 nm and 750 nm. Reflectivity measurements were calibrated against a commercial aluminium standard.

Transfer matrix method. We employ a transfer matrix method described by Heavens[29] and successfully applied to various systems[17,30]. More information can be found in section S5 of the Supplementary Information.

Nanoscale patterning of continuous films and pixels. Patterns are generated by converting a selected greyscale image into a spatially resolved voltage pattern. An Asylum Research MFP-3D atomic force microscope equipped with an ORCA accessory (modified to sustain our higher currents) and a conductive tip (DDESP, Bruker) is used as a nanoscale tip to electrically render several images on both films and pixels as shown in Fig. 2a.

Received 15 January; accepted 13 May 2014.

1. Wuttig, M. Phase-change materials—towards a universal memory? *Nature Mater.* **4,** 265–266 (2005).
2. Lankhorst, M. H. R., Ketelaars, B. W. S. M. M. & Wolters, R. A. M. Low-cost and nanoscale non-volatile memory concept for future silicon chips. *Nature Mater.* **4,** 347–352 (2005).
3. Chen , Y. C. *et al.* Ultra-thin phase-change bridge memory device using GeSb. *2006 International Electron Devices Meeting (IEDM 2006)* http://dx.doi.org/10.1109/IEDM.2006.346910 (2006).
4. Raoux, S. *et al.* Phase-change random access memory: a scalable technology. *IBM J. Res. Develop.* **52,** 465–479 (2008).
5. Caldwell, M. A., Jeyasingh, R. G. D., Wong, H. S. P. & Milliron, D. J. Nanoscale phase change memory materials. *Nanoscale* **4,** 4382–4392 (2012).
6. Ohno, E., Yamada, N., Kurumizawa, T., Kimura, K. & Takao, M. Tegesnau alloys for phase-change type optical disk memories. *Jpn. J. Appl. Phys.* **28,** 1235–1240 (1989).
7. Afonso, C. N., Solis, J., Catalina, F. & Kalpouzos, C. Ultrafast reversible phase-change in GeSb films for erasable optical storage. *Appl. Phys. Lett.* **60,** 3123–3125 (1992).
8. Wuttig, M. & Yamada, N. Phase-change materials for rewriteable data storage. *Nature Mater.* **6,** 824–832 (2007).
9. Kats, M. A., Blanchard, R., Genevet, P. & Capasso, F. Nanometre optical coatings based on strong interference effects in highly absorbing media. *Nature Mater.* **12,** 20–24 (2013).
10. Oosthoek, J. L. M. *et al.* Evolution of cell resistance, threshold voltage and crystallization temperature during cycling of line-cell phase-change random access memory. *J. Appl. Phys.* **110,** 024505 (2011).
11. Loke, D. *et al.* Breaking the speed limits of phase-change memory. *Science* **336,** 1566–1569 (2012).
12. Wang, W. J. *et al.* Engineering grains of $Ge_2Sb_2Te_5$ for realizing fast-speed, low-power, and low-drift phase-change memories with further multilevel capabilities. *2012 International Electron Devices Meeting (IEDM 2012)* http://dx.doi.org/10.1109/IEDM.2012.6479143 (2012).
13. Xiong, F., Liao, A. D., Estrada, D. & Pop, E. Low-power switching of phase-change materials with carbon nanotube electrodes. *Science* **332,** 568–570 (2011).
14. Lee, S. H., Jung, Y. & Agarwal, R. Highly scalable non-volatile and ultra-lowpower phase-change nanowire memory. *Nature Nanotechnol.* **2,** 626–630 (2007).
15. Yamada, N. & Matsunaga, T. Structure of laser-crystallized $Ge_2Sb_{2+x}Te_5$ sputtered thin films for use in optical memory. *J. Appl. Phys.* **88,** 7020–7028 (2000).
16. Collings, N., Davey, T., Christmas, J., Chu, D. P. & Crossland, B. The applications and technology of phase-only liquid crystal on silicon devices. *J. Displ. Technol.* **7,** 112–119 (2011).
17. Burkhard, G. F., Hoke, E. T. & McGehee, M. D. Accounting for interference, scattering, and electrode absorption to make accurate internal quantum efficiency measurements in organic and other thin solar cells. *Adv. Mater.* **22,** 3293–3297 (2010).
18. Bichet, O., Wright, C. D., Samson, Y. & Gidon, S. Local characterization and transformation of phase-change media by scanning thermal probes. *J. Appl. Phys.* **95,** 2360–2364 (2004).
19. Satoh, H., Sugawara, K. & Tanaka, K. Nanoscale phase changes in crystalline $Ge_2Sb_2Te_5$ films using scanning probe microscopes. *J. Appl. Phys.* **99,** 024306 (2006).
20. Hamann, H. F., O'Boyle, M., Martin, Y. C., Rooks, M. & Wickramasinghe, K. Ultra-high-density phase-change storage and memory. *Nature Mater.* **5,** 383–387 (2006).
21. Bhaskaran, H., Sebastian, A., Pauza, A., Pozidis, H. & Despont, M. Nanoscale phase transformation in $Ge_2Sb_2Te_5$ using encapsulated scanning probes and retraction force microscopy. *Rev. Sci. Instrum.* **80,** 083701 (2009).
22. Lingley, A. R. *et al.* A single-pixel wireless contact lens display. *J. Micromech. Microeng.* **21,** 125014 (2011).
23. Llordés, A., Garcia, G., Gazquez, J. & Milliron, D. J. Tunable near-infrared and visible-light transmittance in nanocrystal-in-glass composites. *Nature* **500,** 323–326 (2013).
24. Zrenner, E. Fighting blindness with microelectronics. *Sci. Transl. Med.* **5,** 210ps216 (2013).
25. Nam, S. W. *et al.* Electrical wind force-driven and dislocation-templated amorphization in phase-change nanowires. *Science* **336,** 1561–1566 (2012).
26. Redaelli, A., Pirovano, A., Benvenuti, A. & Lacaita, A. L. Threshold switching and phase transition numerical models for phase change memory simulations. *J. Appl. Phys.* **103,** 111101 (2008).
27. Bez, R., Cappelletti, P., Servalli, G. & Pirovano, A. Phase change memories have taken the field. *5th IEEE International Memory Workshop* 13–16, http://dx.doi.org/10.1109/IMW.2013.6582084 (2013).
28. Heikenfeld, J., Drzaic, P., Yeo, J. S. & Koch, T. A critical review of the present and future prospects for electronic paper. *J. Soc. Inf. Displ.* **19,** 129–156 (2011).
29. Heavens, O. *Optical Properties of Thin Solid Films* Ch. 4, 46–95 (Dover, 1991).
30. Pettersson, L. A. A., Roman, L. S. & Inganas, O. Modeling photocurrent action spectra of photovoltaic devices based on organic thin films. *J. Appl. Phys.* **86,** 487–496 (1999).

Supplementary Information is available in the online version of the paper.

Acknowledgements We thank R. Taylor for scientific discussions related to optical spectroscopy measurements. We are grateful to M. Riede for discussions on the modelling aspects of our study. This research was supported by EPSRC via grant numbers EP/J018783/1, EP/J018694/1 and EP/J00541X/2 as well as the OUP John Fell Fund.

Author Contributions All authors contributed substantially to this work. P.H. and H.B. conceived and designed the experiments. P.H. performed the experiments with input from H. B and C.D.W. All authors analysed the data. The manuscript was written by P.H. and H.B. with input from C.D.W.

Author Information Reprints and permissions information is available at www.nature.com/reprints. The authors declare no competing financial interests. Readers are welcome to comment on the online version of the paper. Correspondence and requests for materials should be addressed to H.B. (harish.bhaskaran@materials.ox.ac.uk).